Quaternary International 438 (2017) 68–80

Contents lists available at ScienceDirect

Quaternary International

journal homepage: www.elsevier.com/locate/quaint

Evidence for cosmic airburst in the Western Alps archived in Late Glacial paleosols

W.C. Mahaney [a, b, *], Peeter Somelar [c], Allen West [d], David Krinsley [e], Christopher C.R. Allen [f], Prasanna Pentlavalli [f], Jonathan M. Young [f], James M. Dohm [g], Malcolm LeCompte [h], Brian Kelleher [i], Sean F. Jordan [i], Coren Pulleyblank [i], Randy Dirszowsky [j], Pedro Costa [k]

[a] *Quaternary Surveys, 26 Thornhill Ave., Thornhill, Ontario, L4J1J4, Canada*
[b] *Department of Geography, York University, 4700 Keele St., North York, Ontario, M3J1P3, Canada*
[c] *Institute of Geology, University of Tartu, Tartu, Estonia*
[d] *Geo-Science Consulting, Dewey, AZ, USA*
[e] *Department of Geological Sciences, Eugene, OR, USA*
[f] *Queen's University Belfast, School of Biological Sciences, Belfast, BT7 1NN, UK*
[g] *The University Museum, The University of Tokyo, Hongo 7-3-1, Bunkyo-ku, Tokyo 113-0033, Japan*
[h] *Center of Excellence in Remote Sensing Education and Research, Elizabeth City State University, Elizabeth, NC, USA*
[i] *School of Chemical Sciences, Dublin City University, Glasnevin, Dublin 9, Ireland*
[j] *School of the Environment, Laurentian University, Sudbury, Ontario, Canada*
[k] *University of Lisbon, Department of Geology, Lisbon, Portugal*

A R T I C L E I N F O

Article history:
Received 28 November 2016
Received in revised form
6 January 2017
Accepted 28 January 2017
Available online 6 February 2017

Keywords:
Younger Dryas Boundary (YDB)
Archived airburst sedimentary evidence

A B S T R A C T

Previous evidence for fragments of a cosmic airburst in the Western Alps has been shown to reside in weathering rinds in surface clasts of Late Glacial (LG) (mid-LG-post Allerød) deposits and in Ah horizons of several associated paleosols. In contrast to outlying strata, Younger Dryas (YD) paleosol horizons contain minor reworked airburst evidence that includes melted quartz/pyroxene grains, carbon spherules, glass-like carbon, and with minor differences in microbial populations. New data from LG paleosol profiles show REEs elevated above crustal abundance in several profiles of mid-Late Glacial age, along with elevated Pt concentrations, similar to those found at the YD Boundary in the Greenland Ice Sheet. Pt/Pd ratios that are elevated above background suggest an exogenic influx of Pt from meteoritic ablation and/or airbursts. An increasing number of localities with sedimentary time lines coeval with an airburst (12.8 ka) indicate the event was intercontinental, producing widespread conflagrations archived in local sediment sequences. This is the first instance worldwide in which evidence of the black mat event has been found both in weathering rinds and in paleosols in the Alps, with such information being applicable to reconnaissance beyond Earth such as in the case of Mars.

1. Introduction

Originating on the slopes of Mt. Viso in the Western Alps of France, the Guil Glacier, a major tributary to the Durance Glacier, underwent insolation-forced recession starting ~15 ka, leaving only isolated ground moraine in the lower catchment. Stillstand-event moraines at 2400 m asl attest to a slow-down of glacial recession sometime during the Bôlling-Allerød retreat phase, followed by a cosmic airburst (Mahaney and Keiser, 2013; Mahaney et al., 2013a, 2016a, 2016b), coeval with the widespread YDB (Younger Dryas Boundary) event of 12.8 ka. The airburst often produced a dark layer sometimes called the "black mat", which in the Alps is represented

* Corresponding author. Quaternary Surveys, 26 Thornhill Ave., Thornhill, Ontario, L4J1J4, Canada.
E-mail addresses: arkose41@gmail.com (W.C. Mahaney), psomelar@ut.ee (P. Somelar), allen7633@aol.com (A. West), Krinsley@uoregon.edu (D. Krinsley), c.allen@qub.ac.uk (C.C.R. Allen), ppentlavalli01@qub.ac.uk (P. Pentlavalli), jyoung@qub.ac.uk (J.M. Young), jmd@um.u-tokyo.ac.jp (J.M. Dohm), ml118031@gmail.com (M. LeCompte), brian.kelleher@dcu.ie (B. Kelleher), sean.jordan5@gmail.com (S.F. Jordan), c.pulleyblank@gmail.com (C. Pulleyblank), rdirszowsky@laurentian.ca (R. Dirszowsky), ppcosta@fc.ul.pt (P. Costa).

http://dx.doi.org/10.1016/j.quaint.2017.01.043
1040-6182/

by carbon encrusted grains in rinds and in paleosols. As elsewhere, the affected sediment typically contains high-temperature carbon (charcoal, soot, carbon spherules, glass-like carbon, melted, welded and quenched grains) and is common across Europe and western North America, but less common across eastern North America. In the Alps, this event was followed by rapid change from a negative to positive glacier mass balance, the advance of Younger Dryas ice, and ensuing moraine construction.

The Guil River catchment (Fig. 1) is aligned along a linear fault channeling the headwaters of the Guil River, to the Durance River and eventually into the Mediterranean Sea. Runoff originates on the western slopes of Mt. Viso (3841 m a.s.l.) on the water divide between France and Italy. Evidence for a cosmic airburst that generated the YDB lays ensconced in local weathering rinds bearing melted grains and glassy carbon spherules previously documented by Mahaney and Keiser (2013) and Mahaney et al. (2016b).

The upper catchment is floored with bedrock, moraine, alluvium, talus, protalus, rockfall, solifluction terraces, and a succession of debris flows (Mahaney, 2008). Whereas recessional moraines are non-existent below 2400 m a.s.l. in the lower valley, the effects of glacial activity and recent erosion are evident on the west-facing valley slopes. At and above ~2400 m a.s.l., the recessional moraines indicate rapid retreat of Late Glacial (Würm–Weichselian) Guil ice from the Durance catchment where it had joined the Durance Glacier (terminus near Sisteron (44° 20′N, 5° 93′E). This is not to say that stillstands of Late Glacial (mid-LG) ice did not occur below ~2400 m a.s.l., but only that if recessionals were emplaced they were short-lived and destroyed, and/or obscured by fluvial erosion as the ice melted and receded. Some carbon in successional stage vegetation, originally present in the Late Glacial soil/parent materials (Ah/C/Cu and C/Cu profiles resident prior to airburst) (Mahaney and Keiser, 2013; Mahaney et al., 2013a), is probably preserved in the paleosols described below. As the Allerød climate episode progressed, the early successional stage alpine grassland of the time (mid-Late Glacial) was probably wet tundra (Mahaney and Keiser, 2013; Mahaney et al., 2013a, 2016a). When the high-temperature cosmic airburst (YDB) descended upon the study area, previously hypothesized by Mahaney et al. (2016a), most life was likely destroyed, with carbon either volatilized, charred, or left as carbon spherules in resident soils (now paleosols), and as opaque carbon in weathering rinds. Some microbes, given various ecological niches in which they thrive, may have survived this event, to finally reside either in weathering rinds or soils later transformed with changes from cold to warmer climates into paleosols. It is conceivable that these 'ancient' bacteria may have left their mark on the present-day metagenome record. The various local lithologies were melted, reformed, and welded into multifarious forms as described below. However, since no impact crater has been identified, it is likely the theorized cosmic event was caused by an airburst fragment emanating from Earth's encounter with the Encke Comet (12.8 ka) (Napier, 2010) thereafter exploding over the Mt. Viso area. The Earth/comet impact is thought to have centered over southern Manitoba, remnants of the impact encountering Earth as the Taurid meteors, which in the early stage-12.8 ka to ~11 ka, were possibly of sufficient mass to maintain positive glacial mass balances in various alpine localities in North and South America and in the Alps, thus sufficient to sustain the YD glacial resurgence linked to the main cosmic event.

Nested recessional mid-LG stillstand moraines at ~2400 m a.s.l., located approximately 1 km from the drainage divide at ~3000 m a.s.l. (Col de la Traversette, Fig. 1), were overrun by a readvance, presumed to be of YD age (sites G1 and G2, Fig. 1) (Mahaney et al., 2016a). Because weathering histories, and hence, paleosols in clastic debris of these mid-LG and YD deposits are similar in depth and other properties, they are considered to have ages separated by centuries or possibly up to a millennium, at best. Whether mid-LG ice

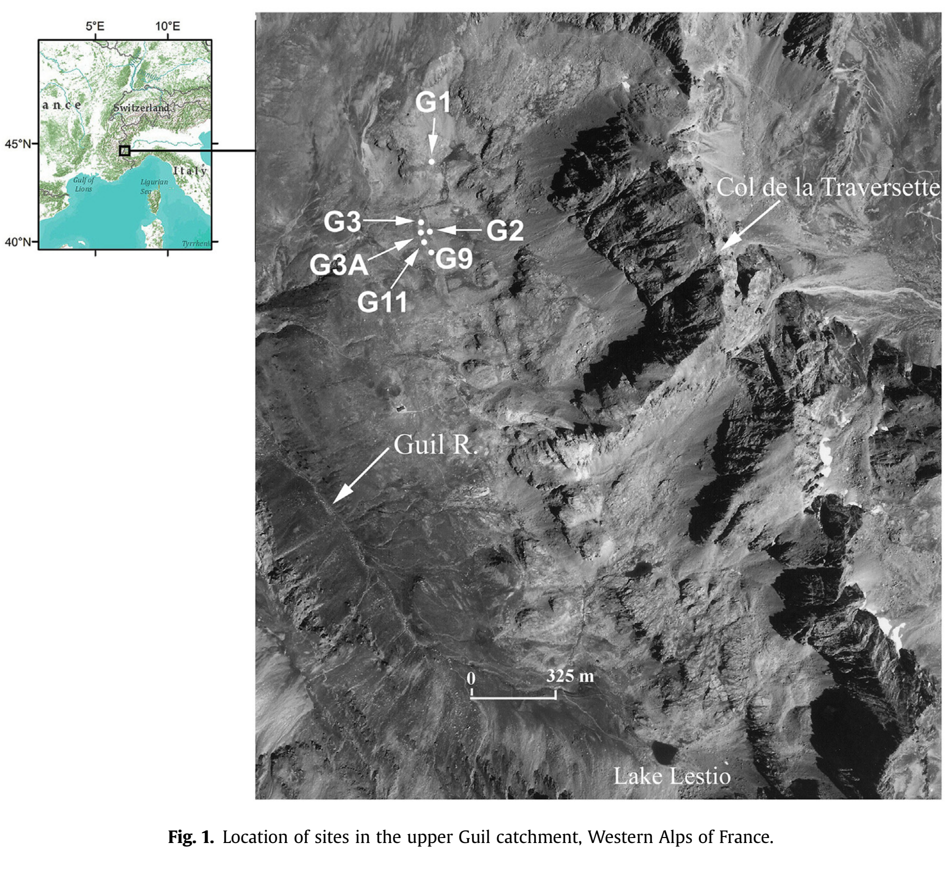

Fig. 1. Location of sites in the upper Guil catchment, Western Alps of France.

remained in the Traversette cirque or disappeared prior to the YD is unknown, but it is unequivocal that YD ice advanced to ~2525 m a.s.l., overrunning any inner mid-LG recessional moraines and occupying a stillstand position for an indeterminate amount of time.

During glacial recession at the end of the last glaciation, ice retreated up the Guil valley toward Mt. Viso, the valley glacier dividing into separate streams, one retreating into the Col de la Traversette cirque, and another retreating into an unnamed cirque near Lac Lestio (2510 m) located below the western summit of Mt. Viso (Fig. 1). Retreat of ice during the Bølling-Allerød interstadial exposed the valley and surrounding area, first to warm/humid conditions (Thiagarajan et al., 2014), followed at the YD boundary (YDB; 12.8 ka) by near instantaneous firing that would have carbonized all or most initial tundra vegetation and incipient soil development. Thus, these fired mid-LG stillstand recessional moraines provided host material for weathering and soil development (Mahaney et al., 2013a) with most deposits still containing residual evidence of a cosmic airburst. With the onset of YD cooling and reversal of the glacial mass balance in the upper valleys, the situation reversed causing a glacial advance and production of a push moraine complex at ~2525 m. Since the YD is the latest climatic reversal during the insolational warming of the Late Glacial record (Ralska-Jasiewiczowa et al., 2001; Gibbard, 2004), moraines emplaced during the event need to be studied for composition and compared with earlier LG deposits.

The YDB airburst event is hypothesized to have triggered the YD cooling episode at ~12.8 ka, the end of a warming trend that started at 14.7 ka (Vanderhammen and Hooghiemstra, 1995; Teller et al., 2002; Lowe et al., 2008), and perhaps earlier (Thiagarajan et al., 2014). The hypothesized cosmic impact or airburst event (Wittke et al., 2013), which could have generated the YD reversal, is still debated in the literature (Firestone et al., 2007; Kennett et al., 2007, 2009; Pinter and Ishman, 2008; Haynes, 2008; Ge et al., 2009; Mahaney and Keiser, 2013; Kennett et al., 2015). Recent critical reviews of the YDB event espoused by Vanderhammen and Van Geel (2008) argued that the wildfires at the YD onset don't require an airburst, and similarly, Broecker et al. (2010) argued that YD climate change doesn't require an airburst. However, neither group provided evidence to refute an airburst. Meltzer et al. (2014) argued that most dates documenting the YDB are not isochronous, but this has been refuted through a Bayesian analysis by Kennett et al. (2015), who showed that widespread YDB layers are coeval within the dating uncertainties. Others argue that the YDB airburst event could not generate a glacial advance lasting over 1 kyr, but this argument may be discounted (Lowe et al., 2008; Teller et al., 2002) because of feedback loops in the thermohaline circulation systems, i.e., once circulation ceased in the North Atlantic, systemic inertia caused a delay of ~1400 years before normal circulation resumed. In addition, Mahaney et al. (2013b) argued that Earth may have experienced a sustained bombardment by fragments of the Taurid Complex following the 12.8 ka airburst (Napier, 2010) that produced a long-term, negative downturn in Earth's heat budget, resulting in a glacial positive mass balance. Here, we present paleosol and weathering-rind information that not only provides supportive evidence of a cosmic airburst over the western Alps and associated Black Mat event, but also provides valuable information for future reconnaissance of Earth and beyond, which includes the Red Planet, Mars.

2. Materials and methods

2.1. Field analysis

Six sites (G = Guil) were selected (Fig. 1) based on field mapping

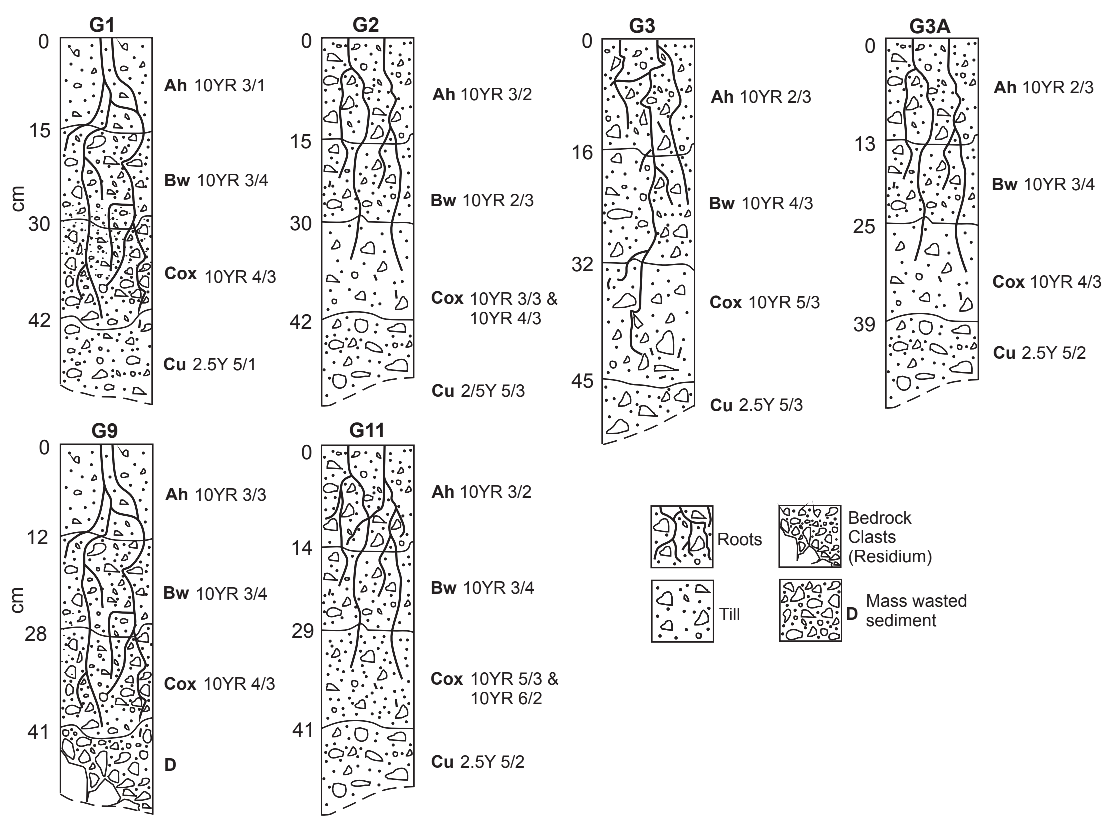

Fig. 2. Paleosol profiles of the Late Glacial stillstand (G3, 3A, 9 and 11) and the Younger Dryas readvance (G1 and G2). The paleosols are all Cryochrepts (SCS, 1999) and show little differences in weathering histories.

and air photo interpretation (1:20,000 scale) of deposits. Clasts embedded in major landform surfaces and profiles (Fig. 2) were sampled after excavating sections to depths of ~0.8 m. Profiles extend to depths of ~40–45 cm ± 5 cm depth. Paleosol descriptions follow standard nomenclature used by the NSSC (1995) and Birkeland (1999). The 'Cox' horizon designation, originally defined by Birkeland (1999), is applied to strata with detectable levels of secondary Fe hydroxides and oxides, whereas 'Cu' refers to unweathered parent material (Hodgson, 1976). The 'Ah' horizon designation is applied when surface color is stronger than 10YR 3/1, an indication of appreciable organic carbon accumulation (Canada Soil Survey Comm., 1998). Soil colors were assigned using Oyama and Takehara's (1970) soil color chips. Bulk samples (250–300 g) were collected from paleosol horizons for particle size, clay mineral, geochemical and microbiological analyses.

2.2. Laboratory sediment analysis

The air dry equivalent of 50 g oven dry material was weighed out for particle size and treated with 30% H_2O_2 to oxidize organic material. After wet sieving the sands (2mm-63 μm), the <63 μm fraction (silt plus clay) was analyzed by hydrometer (Day, 1965). Particle grade sizes follow the Wentworth Scale with the exception of the clay/silt boundary (2 μm) which follows the U.S.D.A. Carbon–Hydrogen–Nitrogen (CHN) analysis was undertaken with a FISONS Instruments NA1500 NCS Series 2 elemental analyzer. The instrument precision was 0.3% RSD (relative standard deviation) or better for C and N and 3.3% RSD for H. Quantification was performed using a certified sulfanilic acid standard (Merck P/N – 100684). Each 8 mg sample, placed in a tin capsule, was combusted at 900 °C with CuO and Cu catalysts. High purity He (Air products BIP) was used as a carrier gas and separation of NO, CO_2, and H_2O was achieved using a PTFE porapak GC column (Porous Polymer Adsorbent). The separation was performed isothermally at 50 °C. Total salts were determined by electrical conductivity. Additional geochemical composition was determined by ICP-AES (Inductively Coupled Plasma Atomic Emission Spectrometry), using a Varian Liberty Series II instrument, with ~1 cm^3 bulk samples first subjected to an aqua-regia digestion. Rare Earth Elements (REEs) were determined by Instrumental Neutron Activation performed on the <177 μm (80 mesh) fraction at Activation Laboratories, Ancaster, Ontario.

The clay fraction was studied for mineral composition by means of powder XRD using a Bruker 8D diffractometer with Ni-filtered CuKά radiation. Scanning steps for oriented samples were 0.02° 2θ from 2 to 55° 2θ. A semi-quantitative mineral composition was determined from peak integral intensities of chlorite, illite-vermiculite, mica + illite, kaolinite, talc and smectite, multiplied by factors of 1, 0.35, 2, 1.4, 0.2, 0.2, respectively (Kalm et al., 1997).

Metagenomic analysis of selected samples follows protocols described for Denaturing gradient gel electrophoresis (DGGE) in Mahaney et al. (2013a) and for later functional gene analysis in the metagenome/transcriptome from this same sample group follows procedures outlined in Mahaney et al. (2016a).

3. Results

3.1. The profiles

The profiles are all Inceptisols (Cryocrepts). The unweathered (Cu) horizons in all six profiles range in colors from 2.5Y 5/1 to 2.5Y 5/3 (from yellowish gray, through dark grayish yellow, to yellowish brown between both sets (YD to mid-LG) of the profiles). Within the weathered sediment in the profiles, colors shift from 10YR 4/3, 5/3 in the Cox horizons, to 10YR 3/4, 4/3 in the Bw horizons, and 10YR 2/1, 2/3 in the Ah horizons, color values and chroma becoming darker upward into the zone of maximum biological activity.

The field textures of all LIA (Little Ice Age) profiles (Mahaney et al., 2016a) range from a pebbly loamy sand to sandy loam (clay <2–4%) supporting structureless (massive) matrices of loose moist consistence and non-sticky and non-plastic properties. Roots are present throughout these profiles with diameters of 2–4 mm. These younger profiles (described by Mahaney et al., 2016a) are probably similar to the soils in existence at the time of the airburst and subsequence conflagration.

Within the G1-G2 (YD) group of paleosols, total thickness is uniform at ~42 cm. The Ah horizon thickness in G1-G2 ranges from 15 to 16 cm (Table 1). Profile thickness in G3 to G11 (mid-LG group) varies from 39 to 45 cm. Soil color in the Ah horizon of the mid-LG and YD groups varies by only one or two value/chroma (Oyama and Takehara, 1970 and Fig. 2). The Bw horizons vary in color by up to one chroma, from brownish black to dull yellowish brown and dark brown. The epipedon and sub-epipedon horizons, as described above, are indicative of minor variable oxide/hydroxide release and indicate similar weathering states in both groups of paleosols. Soil structure grades downward from granular to weak granular in the Ah horizons, to weak blocky structures in the Bw horizons and massive structure in the C horizons of all profiles. Consistence ranges from very friable to loose in all six profiles and depends upon clay content (see Table 1). Non-plastic and non-sticky properties are common throughout all profiles. Roots are generally thin ranging from 2 to 5 mm in diameter and reaching variable depths as shown in Fig. 2. On the basis of profile properties, there is no recognizable difference in age, other than the presence of melted/welded quenched grains in the mid-LG and lack of such in the YD group.

3.2. Particle size

Particle size distributions (Table 1) range across the coarse texture spectrum (from loamy sand and sandy loam to silty loam),

Table 1
Particle size distributions in Late Glacial paleosols, Guil Valley, France.

Site	Horizon	Depth (cm)	Sand (2mm-63μm)	Silt (63-2 μm)	Clay (<2 μm)	Mean *phi*[a]
Late Glacial						
G3	Ah	0–16	52.4	45.2	2.4	3.3
	Bw	16–32	34.8	63.0	2.2	4.6
	Cox	32–45	53.8	45.0	1.2	3.3
	Cu	45+	72.2	27.5	0.3	2.2
G3A	Ah	0–13	66.4	32.4	1.2	2.8
	Bw	13–25	59.5	39.3	1.2	2.6
	Cox	25–39	67.0	31.8	1.2	2.5
	Cu	39+	47.2	51.6	1.2	4.3
G9	Ah	0–12	69.1	30.8	0.1	2.6
	Bw	12–28	71.9	28.0	0.1	2.4
	Cox	28–41	79.2	20.3	0.5	1.7
	D	41+				
G11	Ah	0–14	68.0	31.9	0.1	2.9
	Bw	14–29	48.5	50.2	1.5	3.8
	Cox	29–41	63.7	36.2	0.1	2.9
	Cu	41+	65.1	33.6	1.3	2.9
Younger Dryas						
G1	Ah	0–15	72.6	25.5	1.9	1.8
	Bw	15–30	78.7	16.9	4.4	1.7
	Cox	30–42	71.4	26.0	2.6	2.2
	Cu	42+	57.2	40.2	2.6	3.1
G2	Ah	0–16	48.6	46.2	5.2	3.6
	Bw	16–30	60.2	41.1	2.7	2.9
	Cox	30–42	45.9	51.4	2.7	2.0
	Cu	42+	58.3	39.0	2.7	3.1

[a] Mean phi = Σ25th + 50th + 75th %/3.

which indicates a detrital pattern in the parent material of either sandy silt or silty sand following the Link system (Link, 1966). The theorized cosmic-airburst profiles (G3, 3A, 9 and 11) all lack silt caps, as such, although there is evidence of downward silt translocation in the profiles. Silt caps (plus 5–10%) are present in the Ah horizons of the YD group (G1 and G2). Silt caps, first recognized by Nelson (1954), are utilized as age-indicators (summarized by Birkeland, 1999), and have been used by many workers, to measure aeolian redistribution of glacially-ground material following glacial retreat, as well as to separate soils in soil stratigraphic sequences as indicated here. There is considerable variation in the percentage of silt in the lower epipedons (Bw horizons) of the mid-LG and YD profiles. Younger profiles with weathering initiated following the YD would have had a shortened time frame for the incorporation of silt into their profiles and hence, less time for translocation down profile. This may explain the difference in silt distribution between the two groups of paleosols. The admixture of aeolian-influxed material with moraine sediment in these profiles is indicated to some degree by increased quartz in profile epipedons observed with the light microscope. One out of the four mid-LG, theorized cosmic-airburst profiles show some movement (2%) of clay down profile from the Ah to the Bw horizons, a translocation effect that is similar to the clay distribution in the YD profiles (G1 and G2), with demonstrated movement only in G1.

The mean phi values in all profiles confirm the fractional particle size raw data and indicate only minor downward clay translocation from Ah to Bw horizons.

3.3. Mineralogy

The results of the clay fraction XRD analysis of the Guil profiles are shown in Fig. 3. The clay fraction is dominated by chlorite with high percentages in all groups. The 10 Å mica/illite minerals are more concentrated in the YD relative to the mid-LG group. The chlorite and mica/illite concentration differences probably reflect variations in bedrock eroded first by mid-LG ice and later by YD ice. The composition of chlorite shows less variation down profile in the mid-LG compared with the YD group that may reflect age or moisture differences between the two sets of samples. The content of 10 Å mica, together with illite, increases from the mid-LG to YD groups, which most likely reflects distance from source rock. In the case of G2-Cox and Cu horizons, only traces of 10 Å mica and illite were detected. The 9.6 Å Na-mica is present only in the G3-Ah (11.9%) and in the G3-Cox (4.1%) horizons. In the G3, G3A, G9 and G11 profiles, the serpentine group mineral antigorite is common (5.9–29.5%); however, in the G1 and G2 profiles, it is absent. The mixed-layer, illite-vermiculite is present in the G3 (from trace to 1.5%) and G2 (in Cu, Cox and Ah (1.5–2.6%) profiles and in the Bw horizon (35.2%). Less abundant minerals include talc, which is present in both the G2-Cu and G3-Cu horizons (3.4–4.1%), and smectite in the G1, G2 and G3 Cu horizons (0.6–19.2%). The clay mineral distributions depict a detrital rather than pedogenic origin and offer few clues as to the effect of a cosmic airburst.

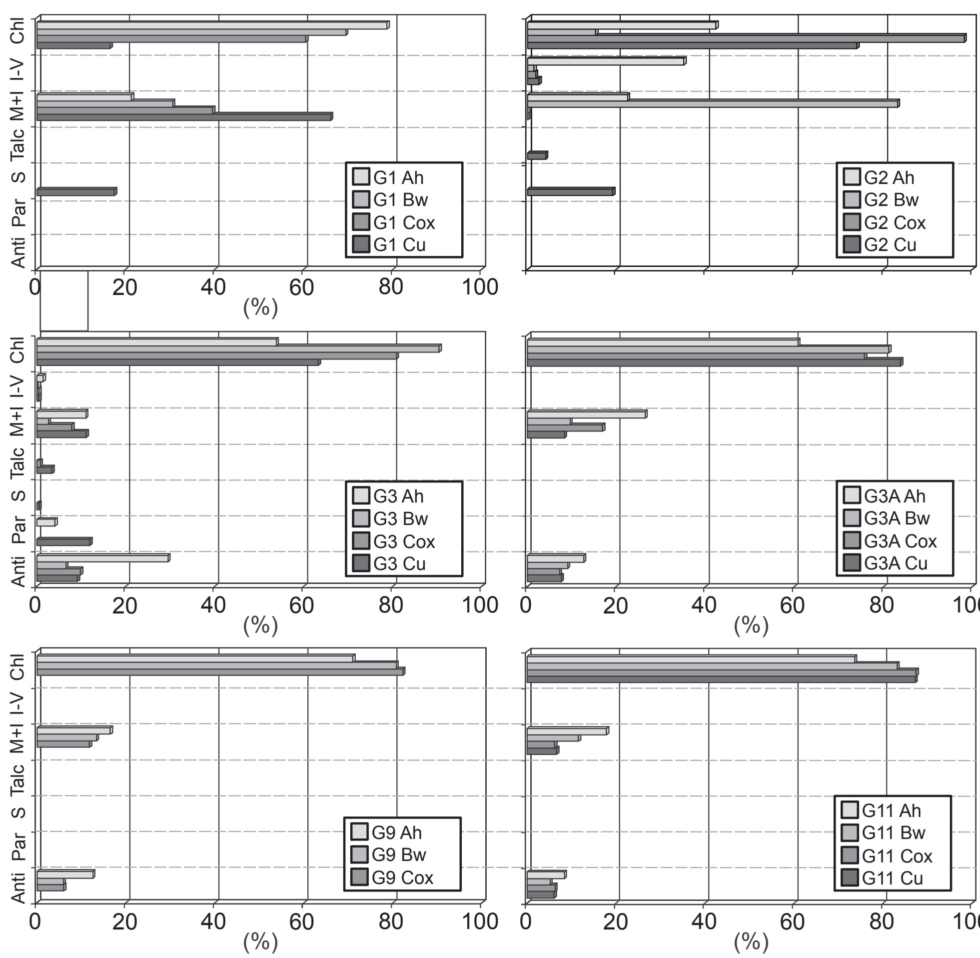

Fig. 3. XRD of the Late Glacial and Younger Dryas paleosols in the upper Guil catchment, Western Alps of France.

3.4. Chemistry

Selected chemical properties (Table 2) were analyzed to determine if differences exist between the two paleosol groups. The data indicate lower than normal organic carbon and nitrogen for Inceptisols in all profiles, which may relate to the time span between collection and analysis. The level of organic carbon (~2%–~7%) may reflect the sandy-silty loam textures of these mid-LG-YD profiles and appreciable moisture. Because the organic carbon steady state of ~5% is reached within middle Neoglacial time (~3 kyr) (Mahaney et al., 2016a), the mid-LG to YD organic carbon variations in these older paleosols are indicative of microclimatic variations on older moraine surfaces. The pH follows this trend with acidity inversely related to organic carbon and indicating little transport of H+ ions within both groups of paleosols. Electrical conductivity (total salts) measurements is relatively low throughout the mid-LG profiles, increasing somewhat in the YD group. The normal inverse relationship between pH and total salts is not observed in either sample group.

Chemical elemental totals, previously published for the G1 and G2 (YD), and G3 (mid-LG) profiles (Mahaney et al., 2016a), were used to assess lithologic and plant inputs relative to postglacial weathering in both the mid-LG (theorized airburst site; G3) and reworked YD sediment (G1 and G2). These data provide elemental concentrations used to gain the buildup of Fe, Mn, and P cycling as related to bacterial numbers and bacteria community development in the two paleosol groups. Low Al concentrations reflect the local metabasalt bedrock that contributed mainly pyroxene and Ca-plagioclase to glacial drift. Relatively high, but fluctuating concentrations of Ca, Na, Mg, and Fe indicate the balancing effects of weathering, leaching, and plant recycling. The Fe content, overall slightly higher in the mid-LG group, reflects a change in source rock from mid-LG to YD, but is not reflected with Mn. Lower Mn concentrations in the Ah horizons of the G1 and G2 profiles, relative to the older paleosols, may be the product of organic or Si dilution, the former from humus and the latter from aeolian input. If organic dilution is the cause, it is hypothesized that higher concentrations of organic carbon in selected horizons might relate to bacterial oxidation of Mn and deposition of MnO_2 (Bougerd and De Vrind, 1987).

To test for variances in chemical weathering across the two discrete groups of paleosols, we used the Chemical Index of Alteration (CIA) (Nesbit and Young, 1982) to determine if an alteration trend could be detected, profile to profile, from the database, despite the relative youth of the paleosols. The CIA is calculated from molar ratios shown in Table 3 of Mahaney et al. (2016a) as follows: $CIA = Al_2O_3/[Al_2O_3 + CaO + Na_2O + K_2O] \cdot 100$, to determine if rates of removal of Ca, Na, and K (major soluble refractory oxides) relative to Al_2O_3 (insoluble) could aid in the detection of a weathering trend (relative values range from 0 to 100). Similar weathering indices have been used in the past, including combinations of elemental concentrations relative to Al or Ti as insoluble elements, or elemental ratios (e.g. Na/Al, Ca/Al, Na/Ti and Ca/Ti) providing simple two-element tests of leaching over variable time frames in both soils and paleosols in various other alpine chronosequences (Hancock et al., 1988; Earl-Goulet et al., 1997).

The CIA weathering index values clearly show slight changes within the profiles and, given the estimated slight age difference, practically no difference between the two groups. However, CIA values are either slightly higher in some Ah horizons, declining slightly with depth, or of uniform value throughout the profile. All values are within the normal range of fresh basalt, at the low end of the weathering scale (Bahlburg and Dobrzinski, 2011). As with profile characteristics and particle size distributions, there is little in the CIA index to suggest a major difference in age between the mid-LG and YD paleosols.

Rare earth elements (REEs, Table 3), which include La, Ce, Nd, Sm, Eu, Tb, Yb, Lu, and Th, were evaluated at the mid-LG sites (G3, 3A, 9 and 11) to test for the potential effects of the theorized YDB airburst event. Several of the heavy REEs (Eu, Tb, Yb, and Lu) were found to be elevated above normal crustal abundance (Rudnick and Gao, 2003) throughout the mid-LG profiles, whereas the remaining four light REEs were found at or below crustal averages in several horizons. Confirmation of this anomalous REE signature was previously noted in the G3 profile (Mahaney et al., 2016a and similar elemental abundances have been reported from reckoned impact/airburst beds at other YDB sites in three countries on two continents, including Blackwater Draw, New Mexico; Murray Springs, Arizona; Lake Hind, Manitoba, Canada; Lommel, Belgium; and Topper, South Carolina (Firestone et al., 2010; Mahaney et al.,

Table 2
Selected paleosol chemical properties of designated cosmic impacted paleosols, Guil catchment, French Alps.

Impacted Sites	Horizons	Depth (cm)	Organic C (%)	H (%)	N (%)	pH (1:5)	E.C. (S/cm)
G3	Ah	0–16	2.43	0.55	0.10	4.90	173.8
	Bw	16–32	1.11	0.37	0.02	4.71	170.5
	Cox	32–45	0.38	0.26	0.04	5.03	151.3
	Cu	45+	0.28	0.28	0.01	4.84	152.4
G3A	Ah	0–13	6.98	1.39	0.55	4.67	131.6
	Bw	13–25	1.91	0.66	0.14	4.80	122.5
	Cox	25–39	0.80	0.44	0.05	4.73	105.2
	Cu	39+	0.27	0.39	nil	4.92	136.5
G9	Ah	0–12	3.17	0.74	0.19	5.33	135.7
	Bw	12–28	0.95	0.50	0.07	5.11	145.6
	Cox	28–41	0.58	0.44	0.05	5.24	123.1
G11	Ah	0–14	5.21	1.14	0.38	5.04	143.7
	Bw	14–29	1.89	0.62	0.14	4.92	136.1
	Cox	29–41	0.84	0.46	0.06	4.92	111.9
	Cu	41+	0.84	0.46	0.06	4.99	118.6
Controls							
G1	Ah	0–15	3.41	0.64	0.08	4.54	265.4
	Bw	15–30	2.99	0.53	0.05	4.54	159.2
	Cox	30–42	0.60	0.29	0.00	4.42	180.9
	Cu	42+	0.62	0.27	0.02	4.72	132.4
G2	Ah	0–16	2.09	0.51	0.03	4.69	225.7
	Bw	16–30	2.56	0.58	0.06	4.37	197.1
	Cox	30–42	0.54	0.33	0.00	4.48	156.2
	Cu	42+	0.48	0.29	0.02	4.64	136.6

Table 3
REEs, Pt, Pd and Pt/Pd ratios in cosmically-impacted Late Glacial and YD paleosols, Guil River catchment, Western Alps.

Site	Horizon	La ppm	Ce ppm	Nd ppm	Sm ppm	Eu ppm	Tb ppm	Yb ppm	Lu ppm	Th ppm	Pt ppb	Pd ppb	Pt/Pd
Late Glacial													
G3	Ah	14.1	36.0	26.0	4.9	2.2	1.9	2.3	0.11	3.5	1.3	1.3	1.0
	Bw	9.9	26.0	18.0	5.0	2.1	0.5	2.5	0.10	2.3	2.2	0.6	3.7
	Cox	7.7	25.0	19.0	4.6	1.8	0.5	2.5	0.11	1.1	1.2	0.6	2.0
	Cu	5.4	23.0	9.0	4.4	1.9	1.3	2.5	0.12	<0.5	–	–	–
G3A	Ah	15.6	35.0	<5	3.4	1.0	<0.5	2.2	0.39	3.9	2.1	0.9	2.3
	Bw	9.1	28.0	15.0	3.8	1.0	<0.5	2.8	0.43	1.6	<0.5	0.7	0.7
	Cox	9.9	31.0	8.0	4.0	0.9	<0.5	3.1	0.43	2.5	<0.5	0.5	1.0
	Cu	8.0	27.0	10.0	4.0	1.2	<0.5	3.1	0.54	1.5	<0.5	<0.5	1.0
G9	Ah	10.8	22.0	12.0	3.2	1.2	<0.5	2.4	0.26	2.9	2.2	0.7	3.1
	Bw	9.2	22.0	14.0	3.6	1.0	1.2	3.2	0.33	1.6	2.4	0.7	3.4
	Cox	8.1	20.0	12.0	3.6	1.6	0.9	3.3	0.33	1.3	1.4	0.7	2.0
G11	Ah	13.6	31.0	16.0	4.0	1.0	<0.5	2.5	0.51	4.3	<0.5	0.6	0.8
	Bw	12.4	32.0	8.0	4.3	1.1	<0.5	3.4	0.49	2.4	15.6	0.6	26
	Cox	8,8	20.0	12.0	3.9	1.1′	0.7	3.1	0.43	1.6	<0.5	0.6	0.8
	Cu	5.7	23.0	9.0	3.9	1.3	0.7	3.3	0.47	1.0	<0.5	<0.5	1.0
Crustal Average		37.1	63.7	27.0	4.7	1.0	0.6	2.0	0.3	10.0	0.5	0.5	
YD Group													
G1	Ah	15.1	34.0	31.0	3.4	1.2	<0.5	2.5	0.21	3.5	<0.3	–	–
	Bw	16.4	28.0	23.0	3.9	0.9	<0.5	2.6	0.30	4.1	0.9	0.8	1.1
	Cox	11.0	23.0	13.0	3.5	1.1	<0.5	2.8	0.28	2.1	0.6	<0.5	1.2
	Cu	7.8	23.0	11.0	3.2	1.3	<0.5	3.1	0.28	1.3	1.7	1.0	1.7
G2	Ah	12.0	29.0	12.0	3.2	0.8	<0.5	2.3	0.22	2.8	–	–	–
	Bw	5.5	18.0	8.0.	2.8	0.9	<0.5	2.5	0.22	0.9	–	–	–
	Cox	5.7	14.0	10.0	3.0	0.8	0.7	2.5	0.23	1.1	1.1	<0.5	2.2
	Cu	3.9	17.0	8.0	2.7	0.8	<0.5	2.5	0.22	0.3	5.4	0.5	10.8

(–) = No detection.

2016a). Several working hypotheses have been invoked to explain these enrichments. These include: (a) normal sedimentary or pedogenic processes that concentrate heavy minerals such as heavy leaching or aquifer transfers; (b) influx of non-local terrestrial ejecta influxed from areas adjoining the proposed YDB impact; (c) arrival of extraterrestrial material contained in the airburst/ impacting body; and/or (d) concentration of solutes from impact-related acid rain. Within the YD group, slightly elevated elements include Eu (in the G1-Ah, Cox and Cu), Tb (in G2-Cox) and Yb (slightly elevated in all horizons of G1 and G2). The stronger suite of elevated REEs, from Sm to Lu within the mid-LG (airburst) group, relative to the slightly elevated concentrations of Eu, Tb and Yb in the YD group, suggest that the valley might have been almost completely free of ice at the time of the YDB, and the scattered REEs within the YD moraine sediment a product of reworking as the ice advanced.

3.5. Black mat airburst evidence

Sedimentary particles in paleosols of mid-LG age (from pebble to silt grade sizes) are found welded with somewhat aerodynamically shaped forms (indicating instantaneous heating and cooling) randomly scattered among sediments showing a normal microtexture indicative of bedrock release followed by glacial, aeolian, and/or fluvial transport. Analyses performed using SEM/ EDS of pebble size clasts show surfaces impacted with fragmental particles, mineral grains forced inward to the clast in groups mimicking phalanx-like structures, and near-surface voids, possibly related to gas release during cooling. The grains in Fig. 4A and B represent elongate hornblende with variable shaped pyroxene, the two principal minerals of the local metabasalt. The large dark areas represent accumulations of opaque carbon. The enlargement shows interbedded fragments of pyroxene for the most part, particles of which may have been taken up during an airburst and welded to carbon sourced from scarce wet tundra at the time of ignition, with the accompanying moisture content no doubt assisting in the volatilization process. The thickness of clast weathering at the time of the hypothesized airburst is estimated to be < 0.5 mm, assuming time of weathering prior to the airburst to be several centuries at most. This estimate of the theorized airburst-effect distance into the clast interior of approximately 0.5 mm is commensurate with or slightly greater than the weakened outer clast area that existed at time of an airburst-generated particle impact/ignition. Weathering of the clast over the <12.8 ka time period has produced a variable coating of Si and Al, partially masking the mineral assemblage exposed in the figures.

Commonly, spheroids are welded together (Fig. 5A) in the suite of paleosol samples studied, whereas others produce a "threadlike" or grapevine of nodules or rod-like forms welded together producing strings of spheroids. These forms are common with black mat encrusted material (Mahaney et al., 2013b). The spheroids shown in Fig. 5A are of variable size ranging from medium to fine silt grade sizes, some nearly entirely melted into a matrix of Al, Si, and O, of which are remnants of former minerals, presumably of terrestrial source. The background matrix of Fig. 5A shows clear evidence of melting and quenching that has presumably removed rough textures expected from mechanically released grains that dominate in glacial terrain, corroborative of a cosmic airburst in the Western Alps, and additional information to the Black Mat enigma. No crystal forms are evident from this image, which is consistent with melting and mixing of heterogeneous material, followed by rapid cooling that did not allow crystallization. Transient high temperatures required for such melting are greater than ~1200 °C (Bunch et al., 2012), well above expected temperatures for natural wildfires in such a sparsely vegetated area. In addition, anthropogenic contamination can be dismissed due to the remoteness of the site, leaving only a cosmic airburst as a plausible explanation.

The EDS (Fig. 5B) shows a mixed chemistry of trace element concentrations with carbon dominating, likely as a glass situated adjacent to multiple spheroids, some nearly entirely buried in the melted matrix. The smooth texture of the spheroids probably resulted from rapid cooling of incoming ejecta from a local airburst and/or from wildfires that generated high concentrations of carbon (soot), followed by condensation of vaporized carbon. The presence

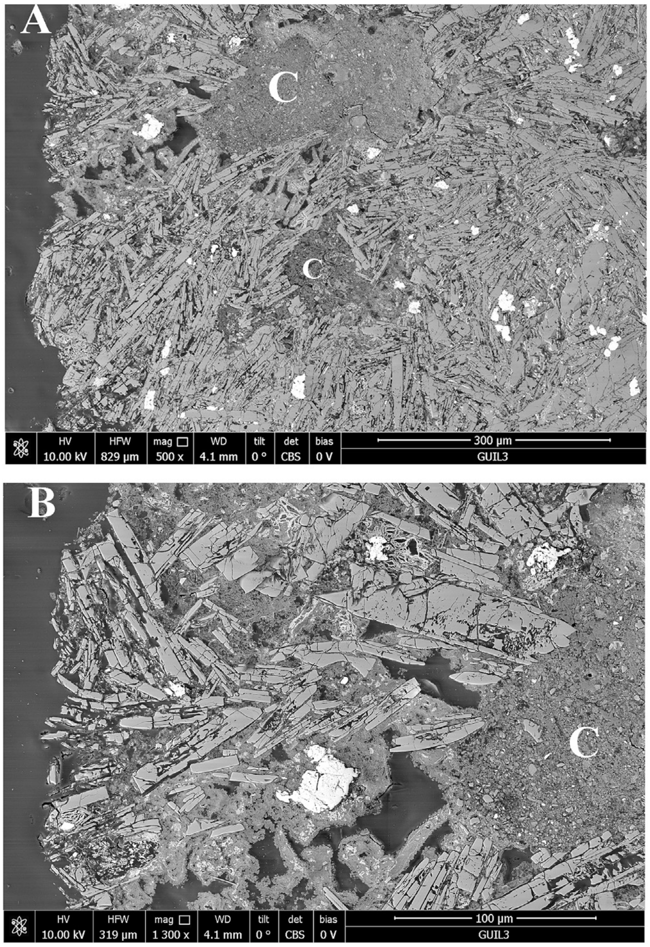

Fig. 4. A, SEM image of a clast embedded in the G3-Ah paleosol showing mineral realignment with kinetic force impacting the pebble surface from left to right producing a phalanx structure with globules of opaque carbon, the upper mass adjacent to void spaces and fragmented outer rind edge. The entire outer ~600 μm of a metabasalt clast was affected by a cosmic airburst that rearranged mineral alignment, melting some and volatilizing others (Mahaney et al., 2016b). Weathering subsequent to impact has produced a ~2 mm thick rind; B, Enlargement of outer rind edge showing detail of the large opaque carbon pool studded with Fe minerals, rearranged amphiboles and melted pyroxene judging by tonal contrast.

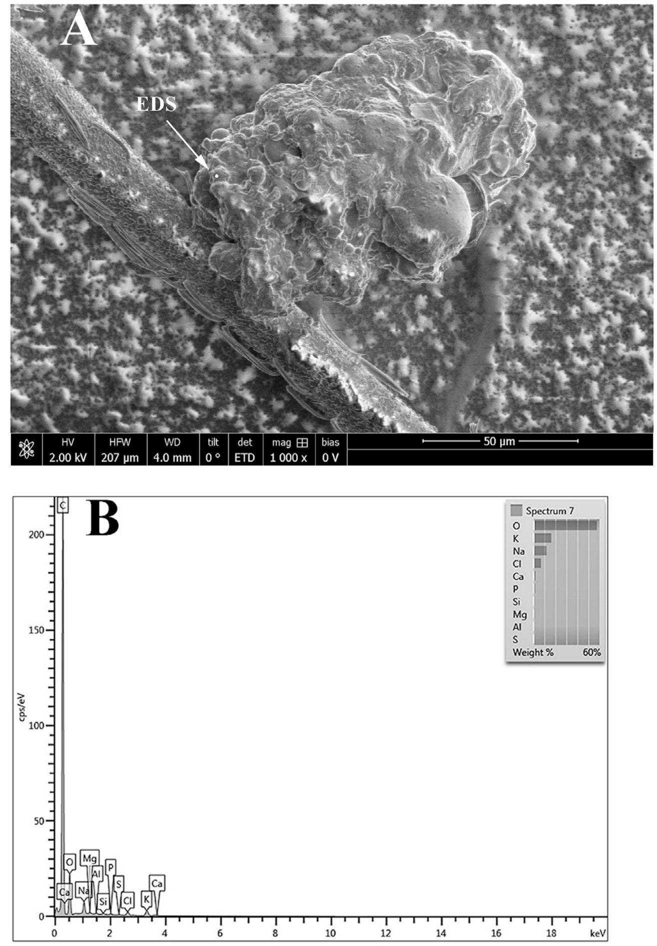

Fig. 5. A, Agglomerate from the G11-Bw horizon showing a wide size range of carbon spherules, welded into a mosaic of Ca and Fe entities. The object displays a variety of different chemistries, depending upon volatilization and cooling/condensation vectors, perfectly preserved as a very fine sand clast; B, EDS of a spherule in A, almost entirely of carbon with minor quantities of volatilized material. The Cl concentration, minor though it is, may indicate probable ion sites in aluminosilicate glass (Stebbins and Du, 2002).

of appreciable Cl (600 ppm; Fig. 5B) may represent ^{35}Cl, as ion sites in aluminosilicate glass, possibly of cosmic origin (Stebbins and Du, 2002), or of terrestrial origin from marine basaltic glass (Van der Zwan et al., 2012).

Other round and/or aerodynamically-shaped particles are present as carbon spherules, commonly 50–250 μm in diameter and found in sediment from the G11 site, especially from the Bw horizon. These spherules are essentially identical to those found in the YDB layer in high quantities at many other sites across several continents (Fig. 6A) (Firestone et al., 2007). At Guil, they sometimes have an aerodynamic, tear-drop shape and most display fragments of detrital minerals that apparently fused to the surface of the carbon spherule when it was molten. These spherules are similar to some particles recovered from the Mucuñuque site (MUM7B) in the northern Andes of Venezuela (Mahaney et al., 2013b), considered to have resulted from instantaneous heating and rapid quenching. One non-spherulitic object, of similar carbon/mineral composition, has a distorted core with disarranged plates of variable size, all welded together (Fig. 6B). A still greater disaggregated welded carbon-rich grain with greater porosity and large fragmental population of silt size particles is shown in Fig. 7. Tonal contrasts indicate grains in the center of the image are probably Fe rich, either pyroxene or amphibolite, possibly olivine. Darker grains on the periphery of the object are plagioclase or opaque carbon glass.

Distributions of Pt/Pd in the two groups of paleosols are shown with respect to crustal averages of meteorite-comet airburst/impact, and alpine PGE-rich rocks (PGE = platinum group elements) in Fig. 8 and Table 3. Within the mid-LG group (G3, 3A, 9 and 11), some horizons are consistent with crustal averages for Pt/Pd, while others, particularly G3-Bw/Cox, G3A-Ah, G9-Ah/Bw, and G11-Bw, are well within the range of a meteorite impact and whereas presumably in this case, an airburst producing extraterrestrial material. The mid-LG G11-Bw horizon has an exceedingly high concentration of Pt, along with a wealth of melted/welded/carbon fused grains as discussed above. The YD group varies considerably, with G1 almost entirely within the range of crustal values for Pt; G2 is similar but with the Cu parent materials registering higher concentrations consistent with the alpine suite of measurements.

4. Discussion

Soil/paleosol morphogenesis across the mid-LG/YD

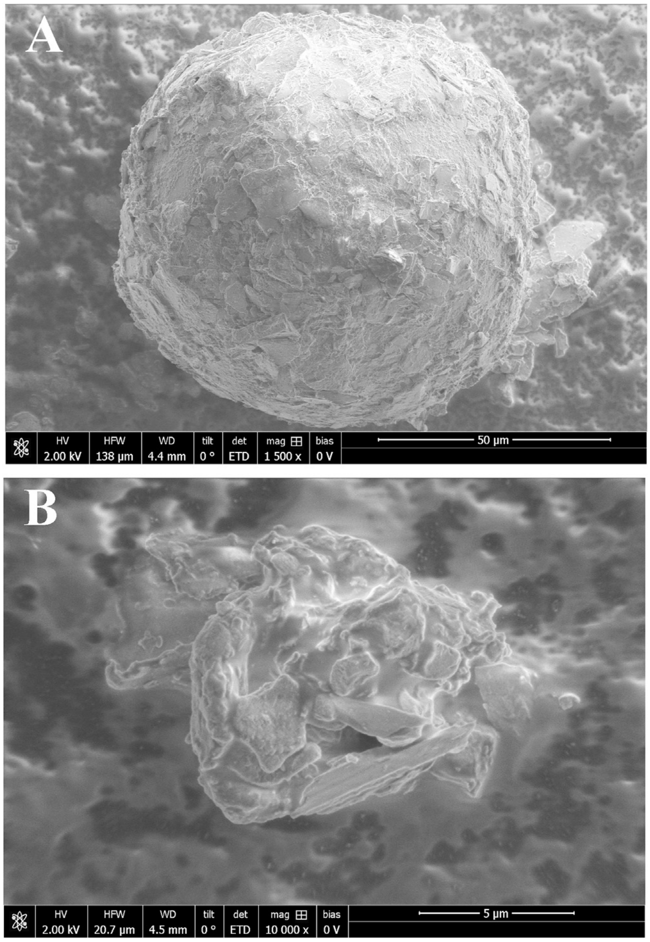

Fig. 6. A, Carbon-rich spherule with partial aerodynamic shaping and pasted-on mineral plates, giving a 'soccer ball' texture similar to grains found in other black mat beds (Mahaney et al., 2013b); B, Deformed carbon-rich object with welded plate-like particles, typical of melting and rapid quenching of plant sap.

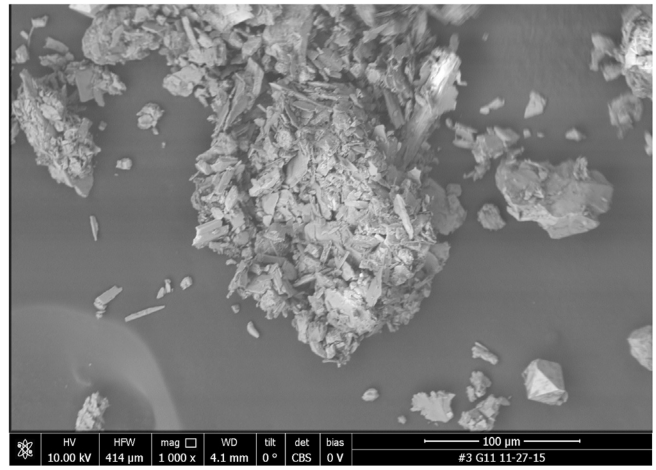

Fig. 7. Wide view of silt size particles of variable dimensions, the center welded agglomerate consisting of many grains with glass like texture, possibly from instant heating and cooling in flight.

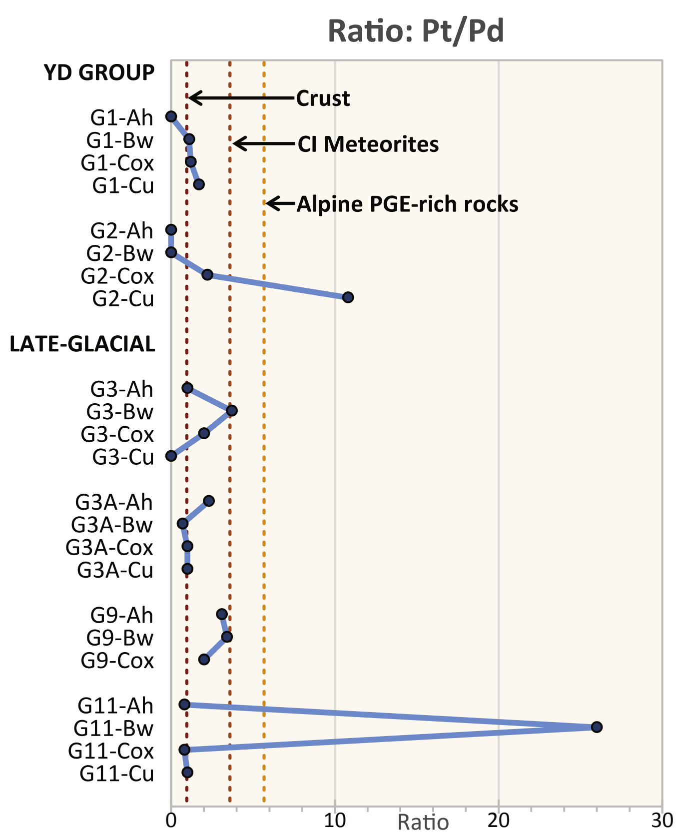

Fig. 8. Pt/Pd ratios across the Late Glacial and Younger Dryas paleosols. Distributions of Pt within the LG paleosols reflect concentrations matching meteorite ablation or airburst distribution, the G3-Bw and G11-Bw registering the highest values. The Pt spike within the G2 profile of YD age possibly represents reworking of older sediment.

chronosequence (~1 kyr) exhibits little difference between the older (G3, G3A, G9, and G11 profiles) and younger (G1 and G2 profiles) given the short time hiatus between deposit emplacement and initiation of weathering (Mahaney et al., 2016a). Changes in sediment/soil color from yellow (2/5Y hue) in the parent substrates (Cu) to yellow-red (10YR hue; Fig. 2) in the weathered sediment (C) shows little variations profile to profile. Upward through the profiles, horizon designation and thickness varies little, with stronger colors showing oxide/hydroxide accumulation in the Bw horizons and organic matter accumulation in the Ah horizon. The older (G3, G3A, G9, and G11 profiles equate with the mid-LG), and younger paleosols (G1 and G2 profiles with the YD) in the sequence, are all considered, on the basis of relative dating methods (Mahaney et al., 2016a), to fall between 11 and 13 ka in age. Among these profiles, the diagnostic Bw horizon, used as a test of age, is consistent in terms of thickness (~15 cm) with near uniform color indicating organic carbon input and overall chemical weathering in an acidic environment. With only slight variance in value and chroma within both profile groups, the Bw hue steadies on 10YR 3/4 and 4/3.

The term black mat refers to a thin black bed of 2–4 cm thickness that results from a suspected conflagration of whatever local surface vegetation consumed by an airburst/impact and associated with melted, aerodynamically quenched, and welded grains that form a separate bed or are mixed with the carbonized layer. In the Alps, it is only the weathering rinds that carry a surface carbonized seam, and welded sands as itemized here, sometimes with carbonized surfaces but lacking the trademark black bed mixed with or overlying a highly modified bed of thermally altered grains. The theorized Andean black mat described by Mahaney et al. (2013b) is a case in point with the affected carbonized sediment overlying and/or mixed with cosmic-airburst grains, dated by radiocarbon, and lying within lacustrine sediment overlain with

Younger Dryas outwash. Unlike the Alps, rinds in the Andean surface deposits date from the end of the YD, and hence, do not carry the cosmic record seen in the Alps (Mahaney and Keiser, 2013).

The hypothesized age of the black mat in the Alps, as discussed here, is based on the relative age of recessional mid-LG deposits carrying hypothesized cosmic-airburst grains, elevated REEs, variable but high Pt/Pd compared with stratigraphically younger YD deposits overlying older mid-LG deposits. Despite the lack of radiocarbon controls in these sediments, the YD/mid-LG succession is hypothesized to equate to the YDB, with an age range of 500 ± yr.

Variable aeolian influx in the mid-LG/YD suite of profiles is indicated by mixed distributions of silt content in the paleosol epipedons (Ah-Bw horizons), relative to that of the subsoil (Cox) and parent materials (Cu). As shown in Table 1, silt content more or less declines upward in G1, increases slightly in the surface horizons of G2, and rises to near ~30 and ~60% in the epipedons (Ah + Bw horizons) of the mid-LG profiles (G3, G3A, G9 and G11) epipedons. While aeolian input is supported by higher quartz contents (allochthonous component inputs) in the Ah group, a test for allochthonous minerals was not undertaken. The increase of silt from G1-G2 (YD age) to the G3-G11 (mid-LG age) group of profiles reflects the retreat area of the spatially expansive Guil/Durance ice during the mid-LG and the release of substantial amounts of glacially-ground sediment. YD ice operating over a much smaller area would be expected to release considerably smaller amounts of glacially-ground material, although the topographic position of each site also probably determines silt input and retention. Reworking of glacially-ground silt by anabatic wind in front of receding ice is probably responsible for these particle size distributions, is not unexpected, and is documented in other areas (Mahaney, 1990; Mahaney et al., 2013c, 2013d).

Clay movement in these paleosols is the exception rather than the rule, with downward translocation of clay apparent only in the G1 and to a lesser extent the G11 profile. Mean phi calculations (Table 1), measuring center-of-gravity shifts in particle size distribution, indicate that down-profile movement is restricted to coarser sediments (hence, lower mean phi values in the Ah to the Bw horizons). Minimal clay translocation down-profile is matched by the lack of organic carbon movement, the one exception being the G2 paleosol where the Bw horizon has been enriched. All other profiles studied show that organic carbon tends to pool in the upper horizons of the epipedons. Moreover, organic carbon measurements horizon-to-horizon are supported by lack of organic films on peds in the Bw horizons.

The secondary/primary mineral distributions in the clay fraction have a purely detrital signature in all profiles, especially with respect to concentrations of chlorite and illite-vermiculite. There is little evidence of clay mineral recrystallization, the data for the most part of which indicates either incorporation of some clay species in the parent material (smectite in profiles G1 and G2, while declining in profile G3 and absent in profiles G3A, 9, and 11) or aeolian delivery (mica + illite in profile G2). Chlorite is generally higher in the parent materials, decreasing up-profile in the other pedons. Because talc is present only occasionally, it is interpreted to be likely sourced from up-valley.

Total Fe concentrations (known only from profiles G1, G2, and G3; Table 3 in Mahaney et al., 2016a) provide little evidence of translocation presumably principally involving ferrihydrite ($5Fe_2O_3 \cdot 9H_2O$, Parfitt and Childs, 1988) as the one partly soluble hydroxide (Mahaney et al., 2013c). While full Fe extract data are not available, it is safe to assume that varying Fe concentrations within the G1 to G3 profiles indicate hydroxide production and little downward movement as in the case of clay and organic materials. Whereas clay movement is seen only in profile G1 (YD) and profiles G3 and G11 (mid-LG), the remaining G2, G3A and G9 profiles lack clay translocation (i.e., the normal soil response of the latter group to soil water loading of profiles), which despite high snowfall in the area appears insufficient to translocate clay size material in half the cases studied.

The physical analysis (including silt cap observations) of the G1- and G2-profile sediments in this study, which appear to confirm the relative young age of these deposits can be considered in light of our previously reported phylogenetic analysis of the same samples using total DNA isolation and 16S rRNA gene pyrosequencing analysis (Mahaney et al., 2016a). The aforementioned Ah to Bw clay translocation (G2 profile) may be reflected in the distribution of the two major eubacterial phyla, Verrucomicrobia and Acidobacteria in the G1 and G2 epipedons. We have previously suggested (Mahaney et al., 2016a) a marked distinction between the role of these groups in these two paleosols as either heterotrophic (Acidobacteria) and autotrophic and/or methanotrophic (Verrucomicrobia) eubacteria components in carbon cycling. A relatively low (<10%) abundance of the heterotrophic Acidobacteria was, as expected, apparent in the G1 profile, representative of a Cox horizon (lower clay relative to Bw). However, in the G2 profile, where variation between the clay content of the Bw and Cox horizons is minimal, a very high (>40%) relative abundance of Acidobacteria is seen in the Cox horizon. In contrast, the autotrophic Verrucomicrobia have extremely high relative abundance (>60%) in the G1-Cox profile/horizon, and markedly lower relative abundance (<20%) in the G2-Cox profile/horizon. Thus, a hypothesis may be presented that suggests a potential link between these two major heterotrophic/autotrophic phyla and silt/clay translocation, some of which may relate to the theorized comet airburst.

Like the DGGE results previously published (Mahaney et al., 2013a) that show a bacteria population variation in the mid-LG paleosols that could relate to an airburst event, the implications from this early database has generated interest to find more data linked to the black mat. In other words, we have a testable approach that could link the black mat to variations both to particle size and to microbial population characteristics. We can speculate that some bacteria would have survived or been modified from an airburst event resulting in very high localized temperature fluctuations, and that the present-day microbial population will be derived from these ancestors. Moreover, variations in the chemical environment of these paleosols presently may – as shown in this study – have resulted in a persistent change in the soil micro-environment, selecting for specific bacterial sub-populations. However, because most developing bacteria DNA at time of the airburst would have been volatilized, we rely on finding modified recombinant DNA from samples that escaped destruction by virtue of niche positions away from the full force of heat and pressure vectors generated by an instantaneous airburst ignition. Even given the low clay content in these mid-LG paleosols, the clay size particles are likely to carry modified bacteria that could be linked to the theorized black mat event. These possibilities could be investigated through comparative studies of the metagenome and meta-transcriptome data associate with these sites, linked to correlation analysis with this chemical meta-data (Thompson et al., 2016).

Moreover, we propose that, when assessing the metagenomic data for these sites, it will be necessary to determine if other physico-mineral-chemical data that differentiate the YD and mid-LG paleosols is reflected in the microbial population structures. The question emerging from the present biogenic/chemical analysis is whether it is possible to actually show (not just hypothesize) that morphogenesis of the mid-LG paleosols is clearly linked to the microbial community structure and/or function, or more specifically whether a cosmic airburst affected the microbial structure in some testable way? Metagenomic analysis by itself makes it possible to test the hypothesis that chemical and physical perturbations resulting from a YDB airburst are reflected in the metagenomic structure of the mid-LG profiles, but are not present in the YD samples. We can frame this in another way: as whether an airburst led to distinct changes in microbial diversity and variation in population structure that is still evident today, even if only as remnant material in random paleosol horizons. In this study, we have presented one specific observation that is certainly testable – that YD sediments with variation in clay content also lead to marked variation in the two most abundant eubacterial phyla in these paleosols. This should now be tested in a detailed study. However, such broad and 'blunt' phylogenetic differences between paleosols may also be accompanied by subtle differences in the functionality of the genes expressed by microbial populations present therein. Only through a complete metagenomic and perhaps transcriptiomic analysis may the full extent of the theorized black mat event on microbial populations and their evolution *in situ* be ultimately appreciated. There is clearly a clustering of microbial populations within the two groups of Inceptisols—mid-LG to YD (Mahaney et al., 2016a), groupings that may or may not be compatible with normal microbe evolution between ~11 and ~13 ka.

Aside from the 16S rRNA DGGE differences in G3-Ah that may relate to a cosmic airburst, previously published by Mahaney et al. (2013a), we do not at the moment detect any differences between the bacterial populations in the Ah, Bw, and C/Cox samples analyzed in the YD and mid-LG Inceptisols outside of the specific clusters (in profiles G1 and G2) mentioned above, and also discussed in Mahaney et al. (2016a). Further studies using functional gene analysis in the metagenome/transcriptome from this same sample group is presently underway and may produce significant results. If the metagenomic analysis employed here is successful it may prove possible to employ similar methods remotely using vehicles like Curiosity to probe the Martian surface where Martian weathering rinds and paleosols likely record extremely ancient (i.e., >4.0 Ga) to more recent Mars environmental and possible exobiological information, as well as possible early solar system and extrasolar conditions. While rinds have not been examined as yet, paleosols have been located by Curiosity and analyzed by Retallack (2014), who considers that full profile (A-C horizons) exists in Gale Crater. He identified a profile in fluvio-lacustrine sediment consisting of A (clay rich) over a B horizon (gypsum rich) with sand cracks, over a slightly weathered C horizon. Limited chemical weathering in Gale Crater rivals similar paleosols acting as proxies in Late Oligocene profiles belonging to the early alpine sequence of moraines near New Mountain Antarctica, albeit without A horizons, profiles revealing at best Cox/C/Cu profiles (Mahaney, 2015; Mahaney et al., 2001).

While weathering rinds on Earth are reported to carry paleoenvironmental records over Late Neogene time (Mahaney et al., 2012), and even to the Late Paleogene (Mahaney and Schwartz, 2016), on Mars the record extends into the Noachian (Mahaney et al., 2012), and likely Hadean-age-equivalent information that has been all but been destroyed on Earth through subduction and plate-tectonic erosion, except for resilient zircons (e.g., Wilde et al., 2001). Because rinds on Mars are so far limited to deep chemical weathering of meteorites (Mahaney et al., 2012), followed by burial and exhumation, followed, in turn, by slower weathering during the Amazonian, instruments aboard the Opportunity Rover were not sensitive enough to measure successive mineral alteration stages related to the two hypothesized time of weathering. Rinds and coatings on Mars are also the subject of identification and analysis by the Curiosity Rover as described by Lanza et al. (2015) who studied the potential of the ChemCan instrument to determine LIBS (Laser-Induced Breakdown Spectroscopy) signatures on rock coatings in Gale Crater. However, the ChemCan instrument has been used to study soil targets in Gale Crater (Cousin et al., 2015) revealing a mix of felsic and basaltic lithologies on surface and buried sediment revealing weathered states. Moreover, despite their probable existence in the Martian record, various rovers have not yet recovered rinds with evidence of former mineral impact or airburst events, although orbiting spacecraft (MRO) have detected glass in an impact crater on Mars (NASA release 6.8. 2015). The weathering rinds, thus, are proposed here to be significant targets of future reconnaissance, not only to yield significant ancient environmental information, which includes impact events, but also possible astrobiological information (Mahaney et al., 2014). Indeed, a reconnaissance by Fink et al. (2013) in the Mojave Desert revealed rinds in sandstone, using an adapter-based imager that offers contextual, multiscale astrobiological imaging that may be appropriate for future Mars missions. The camera used offers scalable imaging that ranges from macroscopic (meters per pixel) to microscopic (micrometers per pixel) imaging, which spans several orders of magnitude revealing weathering, including rind details, on outcrop.

5. Conclusions

The deposit/paleosol stratigraphy in the field area clearly shows two groups of Late Pleistocene paleosols separated by at most ~2 kyr. During the Late Glacial retreat of the Durance-Guil ice, stillstand events produced a double moraine sequence on the flanks of Mt. Viso prior to the hypothesized cataclysmic airburst that may be associated with the theorized and apparent, widely distributed black mat. The outer recessional moraine at ~2400 m occupies a bedrock bar stretching from the present north fork of the Guil River to the south fork, where the ice subsequently thinned to produce two separate glaciers sourced from Traversette to the north and Lake Lestio to the south. The thinning of the north fork valley glacier led to a further stillstand event of unknown duration, with the subsequent mid-LG deposit forming an undulating moraine, part of which is buried by YD moraine. The stratigraphic setting (mid-LG sediment partially overlain with YD moraine) provides proof of a readvance, and the similarity in weathering and paleosol properties between the two groups of paleosols indicates similar relative ages.

When Guil ice receded from 2525 m asl into the Traversette and Lake Lestio cirques, it either expired or was quickly regenerated by the theorized cosmic airburst. It is probable that excessive melting and rapid retreat of ice occurred during the theorized initial airburst, which may explain the flattened crests and cut channels in the mid-LG moraines. However, it is certain that after 12.8 ka, glacier mass balances in the area became positive leading to a readvance of YD ice that constructed moraine complexes in the upper north and south parts of the Guil Valley, a depositional event of which overran part of the mid-LG recessional moraine below the Traversette (documented here), whilst similar events transpired in the catchment below Lake Lestio to the south.

Soil stratigraphic data for the mid-LG and YD moraines reveal a remarkably uniform set of profile mineral and chemical properties between the two groups of deposits, minor differences of which are attributed to micro-topographic and microclimatic variables. Bacteria diversification upward in the profiles is less in both groups of deposits when compared with younger profiles dating from Holocene times (Mahaney et al., 2016a). Geochemical data, specifically the REEs and platinum, indicate variable elemental concentrations relative to crustal average concentrations, with some horizons showing elevated levels compatible with a theorized cosmic impact or more likely hypothesized airburst. Within the LREEs, the mid-LG and YD samples are equal to or less than crustal averages, but within the HREEs, the mid-LG group containing elevated concentrations in some samples, while the YD group of samples is at, slightly above, or well within crustal norms. Thorium is well within the crustal average for both groups of samples. Platinum, on the other hand, is above crustal average in nearly all the mid-LG samples, slightly higher in G1 and lower in G2. These YD samples are probably subject to reworking of sediment produced by the theorized cosmic airburst. The Pt/Pd ratios clearly show the elevated content in the mid-LG sample group, especially in the G11-Bw horizon. Along with Pt, Cl identified randomly, may relate to selected ion sites in aluminosilicate glass, and hence, have a cosmic origin.

Despite the evidence for aeolian-influxed sediment in the Ah horizons, slight variations in the epipedon chemical matrices suggest airfall material that is probably from local sources. Our results have implications beyond possible Earth-perturbing, exogenic-derived events, such as the theorized black-mat event, in that Mars and its accompanying paleosols and weathering rinds have elevated potential to yield not only environmental and possible exobiological records reaching far back into its early evolution (Hadean-age-equivalent to more recent in the Amazonian Period), but also likely early solar system and extrasolar system phenomena.

Acknowledgments

This research was funded by Quaternary Surveys, Toronto. PP was funded by the QUESTOR Center, Queen's University Belfast. BK and SFJ were funded by the Irish Research Council. JY was funded by the Department of Education and Learning, Northern Ireland. DK was supported by instrument use at CAMCOR, University of Oregon, Eugene, Oregon. RD was supported by the Canada Foundation for Innovation. JMD was supported by JSPS KAKENHI Grant Number 26106002 (Hadean BioScience (Grant-in-Aid for Scientific Research on Innovative Areas)), and he expresses his gratitude to the Tokyo Dome Corporation for supporting the TeNQ exhibit and the branch of Space Exploration Education & Discovery, the University Museum, the University of Tokyo.

References

Bahlburg, H., Dobrzinski, N., 2011. A review of the Chemical Index of Alteration (CIA) and its application to the study of Neoproterozoic glacial deposits and climate transitions. In: Arnaud, E., Halverson, G.P., Shields, G.A. (Eds.), The Geological Record of Neoproterozoic Glaciations. Geological Society, London Memoir.

Birkeland, P.W., 1999. Soils and Geomorphology. Oxford University Press, Oxford, UK, p. 430.

Bougerd, F.C., De Vrind, J.M.P., 1987. Manganese oxidation by *Leptothrix discophora*. J. Bacteriol. 169, 489–494.

Broecker, W.S., Denton, G.H., Edwards, R.L., Cheng, H., Alley, R.B., Putnam, A.E., 2010. Putting the Younger Dryas cold event into context. Quat. Sci. Rev. 29, 1078–1081.

Bunch, T.E., Hermes, R.E., Moore, A.M.T., Kennett, D.J., Weaver, J.C., Wittke, J.H., DeCarli, P.S., Bischoff, J.L., Hillman, G.C., Howard, G.A., Kimbel, D.R., Kletetschka, G., Lipo, C.P., Sakai, S., Revay, Z., West, A., Firestone, R.B., Kennett, J.P., 2012. Very high-temperature impact melt products as evidence for cosmic airbursts and impacts 12,900 years ago. Proc. Natl. Acad. Sci. U. S. A. 109, 11066–11067.

Canada Soil Survey Committee (CSSC), 1998. The Canadian System of Soil Classification, 637. NRC Research Press, Ottawa, Canada, p. 187 (Publ. 1646).

Cousin, A., Meslin, P.Y., Wiens, R.C., Rapin, W., Mangold, N., Fabre, C., Gasnault, O., Forni, O., Tokar, R., Ollila, A., Schröder, S., Lasue, J., Maurice, S., Sautter, V., Newsom, H., Vaniman, D., Mouélic, S.Le, Dyar, D., Berger, G., Blaney, D., Nachon, M., Dromart, G., Lanza, N., Clark, B., Clegg, S., Goetz, W., Berger, J., Barraclough, B., Delapp, D., MSL Science Team, 2015. Compositions of coarse and find particles in Martian soils at gale: a window into the production of soils. Icarus 249, 22–42.

Day, P.E., 1965. Particle fractionation and particle size analysis. In: Black, C.A. (Ed.), Methods of Soil Analysis. American Society of Agronomy, Madison, Wisconsin, pp. 545–567.

Earl-Goulet, J., Mahaney, W.C., Hancock, R.G.V., 1997. Geochemistry of spodosols developed in Holocene till, Norra Storfjället Massif, northern Sweden. J. Radioanalytical Nucl. Chem. 219 (1), 7–17.

Fink, W., Sun, H.J., Mahaney, W.C., Kuhlman, K.R., Schulze-Makuch, D., 2013. Planetary imaging in powers of ten: a multiscale, multipurpose astrobiological imager. Astrobiology 13, (11), 1005–1010.

Firestone, R.B., West, A., Kennett, J.P., Becker, L., Bunch, T.E., Revay, Z.S., Schultz, P.H., Belgya, T., Kennett, D.J., Erlandson, J.M., Dickenson, O.J., Goodyear, A.C., Harris, R.S., Howard, G.A., Kloosterman, J.B., Lechler, P., Mayewski, P.A., Montgomery, J., Poreda, R., Darrah, T., Que Hee, S.S., Smith, A.R., Stich, A., Topping, W., Wittke, J.H., Wolbach, W.S., 2007. Evidence for an extraterrestrial impact 12,900 years ago that contributed to the megafaunal extinctions and the Younger Dryas cooling. Proc. Natl. Acad. Sci. 104, 16016–16021.

Firestone, R.B., West, A., Revay, Z., Hagstrum, J.T., Belgya, T., Gue Hee, S.S., Smith, A.R., 2010. Analysis of the Younger Dryas impact layer. J. of the Siberian Federal Univ. Eng. Techn 1 (3), 30–62.

Ge, T., Courty, M.M., Guichard, F., 2009. Field-analytical approach of land-sea records elucidating the Younger Dryas syndrome. In: American Geophysical Union, Abstract PP31D-432.

Gibbard, P.L., 2004. Quaternary…now you see it, now you don't. Quat. Perspect. 14, 89–91.

Hancock, R.G.V., Mahaney, W.C., Stalker, A.MacS, 1988. Neutron activation analysis of tills in the North Cliff section, Wellsch Valley, Saskatchewan. Sediment. Geol. 55, 185–196.

Haynes, C. Vance, 2008. Younger Dryas “black mats” and the Rancholabrean termination in North America. Proc. Natl. Acad. Sci. 105, 6520–6525.

Hodgson, J.M., 1976. Soil Survey Field Handbook — Soil Survey Tech, Monograph, No. 5. 773. Rothamsted Experimental Stn, Harpenden, Herts, p. 99.

Kalm, V., Kriiska, A., Aruväli, J., 1997. Mineralogical analysis applied in provenance studies of Estonian Neolithic pottery. — Eesti TA Toimetised. Geoloogia 1, 16–34.

Kennett, J.P., Becker, L., West, A., 2007. Triggering of the Younger Dryas cooling by extraterrestrial impact. AGU Annu. Mtg 2007. PP41A–05.

Kennett, D.J., Kennett, J.P., West, A., Mercer, C., Que Hee, S.S., Bement, L., Bunch, T.E., Sellers, M., Wolbach, W.S., 2009. Nanodiamonds in the Younger Dryas Boundary Sediment. Science 323 (5910), 94.

Kennett, J.P., Kennett, D.J., Culleton, B.J., Tortosa, J.E.A., Bischoff, J.L., Bunch, T.E., Daniel, I.R., Erlandson, J.M., Ferraro, D., Firestone, R.B., Goodyear, A.C., Israde-Alcántara, I., Johnson, J.R., Jordá Pardo, J.F., Kimbel, D.R., LeCompte, M., Lopino, N.H., Mahaney, W.C., Moore, A.M.T., Moore, C.R., Ray, J.H., Stafford Jr., T.W., Tankersley, K.B., Wittke, J.H., Wolbach, W.C., West, A., 2015. Bayesian Chronological Analyses Consistent with Synchronous Age of 12,835–12,735 Cal B.P. For Younger Dryas Boundary on Four Continents. http://dx.doi.org/10.1073/pnas.1507146112.

Lanza, N.L., Olila, A.M., Cousin, A., Wiens, R.C., Clegg, S., Mangold, N., Bridges, N., Cooper, D., Schmidt, M., Berger, J., Arvidson, R., Melikechi, N., Newsom, H.E., Tokar, R., Hardgrove, C., Mezzacappa, A., Jackson, R.S., Clark, B., Forni, O., Maurice, S., Nachon, M., Anderson, R.B., Blank, J., Deans, M., Delapp, D., Léveillé, R., McInroy, R., Martinez, R., Meslin, P.-Y., Pinet, P., 2015. Understanding the signature of rock coatings in laser-induced beeakdown spectroscotpy, data. Icarus 249, 62–73.

Link, A.G., 1966. The textural classification of sediments. Sedimentology 7 (3), 249–254.

Lowe, J.J., Rasmussen, S.O., Björck, S., Hoek, W.Z., Steffensen, J.P., Walker, M.J.C., Yu, Z.C., 2008. Synchronisation of palaeoenvironmental events in the North Atlantic region during the Last Termination: a revised protocol recommended by the INTIMATE group. Quat. Sci. Rev. 27, 6–17.

Mahaney, W.C., 1990. Ice on the Equator. Wm Caxton Ltd., Ellison Bay, Wisc, p. 386.

Mahaney, W.C., 2008. Hannibal's Odyssey: Environmental Background to the Alpine Invasion of Italia. Gorgias Press, Piscataway, NJ, p. 221.

Mahaney, W.C., 2015. Pedological Iron/Al extracts, clast analysis and Coleoptera from Antarctic paleosol 831: evidence of a middle Miocene or earlier climatic optimum. J. Geol. 123, 113–132.

Mahaney, W.C., Keiser, L., 2013. Weathering rinds: unlikely host clasts for evidence of an impact-induced event. Geomorphology 184, 74–83.

Mahaney, W.C., Schwartz, S., 2016. Paleoclimate of Antarctica reconstructed from clast weathering rind analysis. Palaeogeogr. Palaeoclimatol. Palaeoecol. 446, 205–212.

Mahaney, W.C.,Dohm, Baker, J.M., Newsom, V.R., Malloch, H.E., Hancock, D., Campbell, R.G.V., Sheppard, I., Milner, M.W.D., 2001. MorphogenesisofAntarctic paleosols: Martian analogue. Icarus 154, 113–130.

Mahaney, W.C., Dohm, J.M., Fairen, Alberto, 2012. Weathering rinds on clasts: examples from Earth and Mars as short and long term recorders of paleoenvironment. J. Planet. Space Sci. 73, 243–253.

Mahaney, W.C., Keiser, Leslie, Krinsley, D.H., Pentlavalli, P., Allen, C.C.R., Somelar, P., Schwartz, Stephane, Dohm, Dirzowsky, James M., Randy, Allen, West, Julig, P., Costa, P., 2013a. Weathering rinds as mirror images of palaeosols: examples from the Western Alps with correlation to Antarctica and Mars. J. Geol. Soc. http://dx.doi.org/10.1144/jgs2012-150. Lyell Volume.

Mahaney, W.C., Keiser, L., Krinsley, D., Kalm, V., Beukens, R., West, A., 2013b. New evidence from a black mat site in the northern Andes supporting a cosmic impact 12,800 years ago. J. Geol. 121 (6), 591–602.

Mahaney, W.C., Barendregt, R.W., Hamilton, T.S., Hancock, R.G.V., Tessler, D., Costa, P.J.M., 2013c. Stratigraphy of the Gorges Moraine System, Mount Kenya: palaeosol and paleoclimate record. J. Geol. Soc. http://dx.doi.org/10.1144/jgs2012-079.

Mahaney, W.C., Barendregt, R.W., Hamilton, T.S., Hancock, R.G.V., Costa, P.J.M., 2013d. Soil mineralogy and chemistry of Late Pliocene-Early Pleistocene paleosols on Mount Kenya: age and paleoclimate reconstruction. Geomorphology 204, 217–228.

Mahaney, W.C., Dohm, J.M., Schwartz, S., Findling, N., Hart, K.M., Conway, S., Allen, C.C.R., Miyamoto, H., Fairén, A.G., 2014. Mineralogy, chemistry and biological contingents of an Early-Middle Miocene Antarctic paleosol and its relevance as a Martian analogue. Planet. Space Sci. 104, 253–269.

Mahaney, W.C., Somelar, P., Dirszowsky, R.W., Kelleher, B., Pentlavalli, P., McLaughlin, S., Kulakova, A.N., Jordan, S., Pulleyblank, C., West, A., Allen, C.C.R., 2016a. A microbial link to weathering of postglacial rocks and sediments, Mt. Viso area, Western Alps, demonstrated through analysis of a soil/paleosol bio/chronosequence. J. Geol. 124, 149–169.

Mahaney, W.C., Krinsley, D.H., Razink, J., Fischer, R., Langworthy, K., 2016b. Clast rind analysis using multi-high resolution instrumentation. Scanning 38 (3), 202–212.

Meltzer, D.J., Holliday, V.T., Cannon, M.D., Miller, S.D., 2014. Chronological evidence fails to support claim of an isochronous widespread layer of cosmic impact indicators dated to 12,800 years ago. PNAS. http://dx.doi.org/10.1073/pnas.1401150111.

National Soil Survey Center (NSSC), 1995. Soil Survey Laboratory Information Manual. Soil Survey Investigations Report No. 45. Version 1.00. USDA, Washington, DC., p. 305

Napier, W.M., 2010. Palaeolithic extinctions and the Taurid complex. Mon. Not. R. Astron. Soc. 405, 1901–1906.

Nelson, R.L., 1954. Glacial geology of the Frying Pan river drainage, Colorado. J. Geol. 62, 325–343.

Nesbitt, H.W., Young, G.M., 1982. Early Proterozoic climates and plate motions inferred from major element chemistry of lutites. Nature 299, 715–717.

Oyama, M., Takehara, H., 1970. Standard Soil Color Charts. Japan Research Council for Agriculture, Forestry and Fisheries, Tokyo, Japan.

Parfitt, R.L., Childs, C.W., 1988. Estimation of forms of Fe and Al: a review and analysis of contrasting soils by dissolution and Moessbauer methods. Aust. J. Soil Res. 26, 121–144.

Pinter, N., Ishman, S.E., 2008. Impacts, mega-tsunami, and other extraordinary claims. GSA Today 18, 37–38.

Ralska-Jasiewiczowa, M., Stebich, M., Negendank, J.F.W., 2001. Correlation and synchronization of Lateglacial continental sequences in northern central Europe based on annually laminated lacustrine sediments. Quat. Sci. Rev. 20, 1233–1249.

Retallack, G.J., 2014. Paleosols and paleoenvironments of early Mars. Geology 42 (9), 755–758.

Rudnick, R.L., Gao, S., 2003. Composition of the continental crust. In: Rudnick, Roberta L., Holland, H.D., Turekian, K.K. (Eds.), Treatise on Geochemistry, vol. 3. Elsevier, p. 659, 1-64.

Soil Survey Staff, 1999. Soil Taxonomy. USDA Agric. Handbook No. 436. Gov't Printing Office, Washington, D.C.

Stebbins, J.F., Du, L.-S., 2002. Chloride ion sites in silicate and aluminosilicate glasses: a preliminary study by 35Cl solid state NMR. Am. Mineralogist 87, 359–363.

Teller, J.T., Leverington, D.W., Mann, J.D., 2002. Freshwater outbursts to the oceans from glacial Lake Agassiz and their role in climate change during the last deglaciation. Quat. Sci. Rev. 21, 879–887.

Thiagarajan, N., Subhas, A.V., Southon, J.R., Eiler, J.M., Adkins, J.F., 2014. Abrupt pre-Bølling-Allerød warming and circulation change in the deep ocean. Nature 511, 75–78.

Thompson, L.R., Williams, G.J., Haroon, M.F., Shibl, A., Larsen5, P., Shorenstein, J., Knight, R., Sting, U., 2016. Metagenomic covariation along densely sampled environmental gradients in the Red Sea. ISME J. http://dx.doi.org/10.1038/ismej.2016.99. Advanced online publication.

Van der Hammen, T., Hooghiemstra, H., 1995. The El Abra Stadial, a Younger Dryas equivalent in Colombia. Quat. Sci. Rev. 14, 841–851.

Van der Hammen, T., Van Geel, B., 2008. Charcoal in soils of the Allerød-Younger Dryas transition were the result of natural fires and not necessarily the effect of an extra-terrestrial impact. Neth. J. Geosciences 87, 359–361.

Van der Zwan, F.M., Fietzke, J., Devey, C.W., 2012. Precise measurement of low (<100 ppm) chlorine concentrations in submarine basaltic glass by electron microprobe. J. Anal. Atomic Spectrom. 27, 1066–1974.

Wilde, S.A., et al., 2001. Evidence from detrital zircons for the existence of continental crust and oceans on the Earth 4.4 Gyr ago. Nature 409, 175–178.

Wittke, J.H., Weaver, J.C., Bunch, T.E., Kennett, J.P., Kennett, D.J., Moore, A.M.T., Hillman, G.C., Tankersley, K.B., Goodyear, A.C., Moore, C.R., Daniel Jr., R., Ray, J.H., Lopinot, N.H., Ferraro, D., Israde-Alcántara, I., Bischoff, J.L., DeCarli, P.S., Hermes, R.E., Kloosterman, J.B., Revay, Z., Howard, G.A., Kimbel, D.R., Kletetschka, G., Nabelek, L., Lipo, C.P., Sakai, S., West, A., Firestone, R.B., 2013. Evidence for deposition of 10 million tonnes of impact spherules across four continents 12,800 years ago. Proc. Natl. Acad. Sci. U. S. A. http://dx.doi.org/10.1073/pnas.1301760110.